Absolute Frequency Measurement of ^{6}Li D Lines with khz-Level Uncertainty

Rui Li,[1] Yuelong Wu,[1,*] Yang Rui,[1] Bo Li,[1] Yanyi Jiang,[1,†] Longsheng Ma,[1] and Haibin Wu[1,2,‡]
[1]State Key Laboratory of Precision Spectroscopy, East China Normal University, Shanghai 200062, People's Republic of China
[2]Collaborative Innovation Center of Extreme Optics, Shanxi University, Taiyuan 030006, China

(Received 28 August 2019; accepted 3 December 2019; published 13 February 2020)

We report the precision measurement of the absolute frequencies, hyperfine splitting, and $2P$ fine structure splitting in cold atoms of ^{6}Li. Using the stabilized optical frequency comb and developed heterodyne detection technique, the photon shot-noise limited optical spectroscopy is achieved. The measurement of absolute frequencies of D_1 lines is reached with an uncertainty of about 1 kHz, which is 1 order of magnitude more accurate than previous measurements. The hyperfine splitting of the D_1 line and $2P$ fine structure splitting of ^{6}Li are 26.103 1 (14) and 10 052.780 4 (18) MHz, respectively, in agreement with recent theoretical calculations. Our results could provide a benchmark to test the theory at the higher precision and help to resolve large discrepancies among previous experiments.

DOI: 10.1103/PhysRevLett.124.063002

In recent years there has been a growing theoretical and experimental interest in high precision laser spectroscopy of lithium atoms [1–21]. This is mainly because neutral lithium has a relatively simple three-electronic structure and thus accurate theoretical calculations [5–12] including quantum electrodynamics (QED), isotope shift, and relativistic corrections can be obtained from many-body wave functions. In addition, besides two stable isotopes,[6,7]Li, the lithium atom has three radioactive isotopes, [8,9,11]Li, which have greatly promoted the study of nuclear physics and led to the discovery of the neutron halo [22–24]. The development of high precision spectroscopy of lithium offers a benchmark to such theories and can be used to determine the nuclear radius and measure the fine structure constant, thus testing fundamental physical laws with higher accuracy.

A number of experiments have measured the fine and hyperfine structure splittings as well as the isotope shifts for the D_1 and D_2 lines at optical frequencies for ^{6}Li and ^{7}Li [13–21]. Typically, the fluorescence spectra of a thermal atomic beam excited by a laser are used to measure optical transitions. These data offer an important comparison with the current most accurate calculations for three-electron atoms. However, there are considerable discrepancies in these experimental measurements. In particular, there is a significant discrepancy in measurements of the isotope shifts of the D_1 transitions of Li. Recently, the absolute transition frequencies of lithium atoms are measured with an uncertainty less than 25 kHz by a femtosecond optical frequency comb [20,21]. Although it partially resolves the discrepancies, the inconsistence of the experimental data and the comparison between the data with theory still persists. More accurate atomic spectroscopy and a theory of lithium atoms need to be developed.

Here we report the precision measurement of the absolute frequencies, hyperfine splitting, and $2P$ fine structure splitting of ^{6}Li based on the stabilized optical frequency comb. In contrast to previous measurements with hot atoms in the atomic beams, cold atoms of ^{6}Li and absorption spectra are used for experiments, which cause the smaller Doppler effect. The heterodyne detection technique is developed and the photon shot-noise limited detection of optical spectroscopy is achieved. It greatly improves the signal-to-noise ratio (SNR) and enhances the sensitivity of the measurement. The measurement of absolute frequencies is reached with an uncertainty below 1 kHz, which is one order of magnitude smaller than the previously most accurate measurements. The hyperfine splitting of the D_1 line and $2P$ fine structure splitting of ^{6}Li are 26.103 1(14) and 10 052.780 4(18) MHz, respectively, in reasonable agreement with recent theoretical calculations including QED corrections.

The schematic of the experimental setup is shown in Fig. 1. The method for producing cold atoms of ^{6}Li has been described in our previous work [25,26]. ^{6}Li is cooled from 673 K to about 300 μK with 10^8 atom numbers by using Zeeman slower and the standard magneto-optical trapping (MOT) technique. Since the hyperfine levels in the D_2 line are closely spaced and not resolved, there is generally no sub-Doppler cooling mechanism. We develop the gray molasses [27] of the D_1 line, which further reduces the temperature of the atoms to about 50 μK with 5×10^7 atoms [28]. A magnetic field surrounding the cold atoms is greatly suppressed by the magnetic shield and compensation cage. The residual magnetic field at the interaction region is about 0.8 μT measured by a long pulse two-photon Raman spectroscopy (see Supplemental Material [29]). Two laser beams propagating in opposite directions with perpendicular linear polarizations are used to probe the atoms. The diameters of the probe lights are about 2.6 mm at the location of atoms and the angle

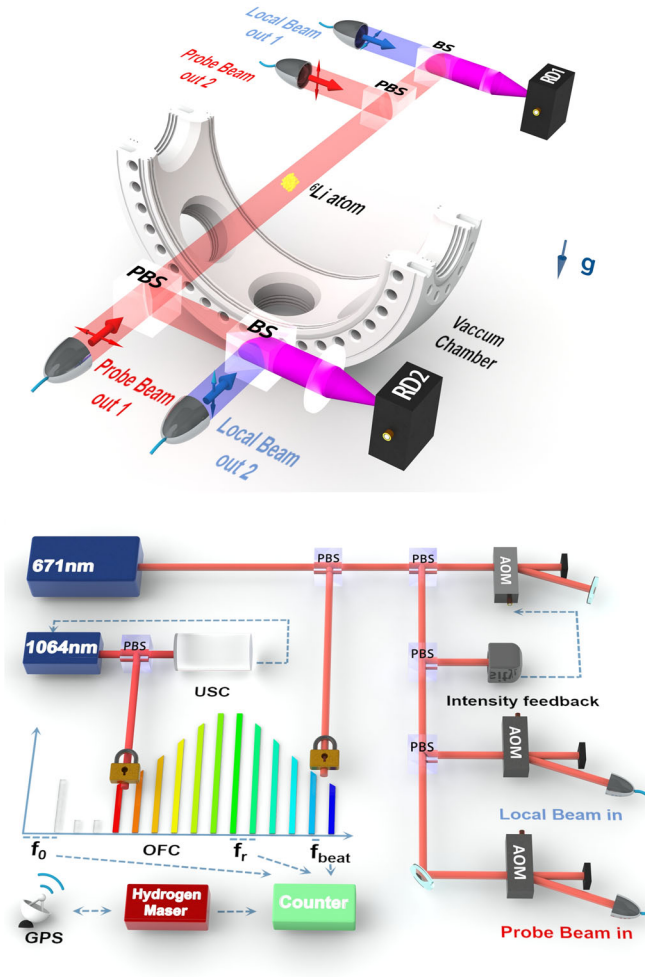

FIG. 1. The schematic of the experimental setup and the heterodyne detection. Optical frequency comb (OFC); ultrastable cavity (USC); global positioning system (GPS); acousto-optic modulator (AOM); resonant photodetectors (RD); polarized beam splitter (PBS). The optical frequencies are measured by an OFC that is based on a femtosecond Ti:sapphire laser (1064 nm) referenced to an USC (the instability is better than 1×10^{-15} at 1 s average).

between two beams is carefully adjusted to better than 200 μrad.

For lighter atoms, the imbalance of light beams could cause the blueshift of the measured frequencies. So the intensity difference between probe beams are controlled below 5×10^{-3}. Their frequencies are directly locked to an optical frequency comb, which is based on a femtosecond Ti:sapphire laser with a repetition frequency $f_r = 998$ MHz. The OFC is referenced to an ultrastable optical cavity, the instability of which is better than 1×10^{-15} at 1 s average. f_r and the initial frequency offset f_0 are referenced to a hydrogen maser, which has a frequency stability of 2×10^{-15} with an integral of more than 1000 s. The hydrogen maser is linked to the Cs atomic clock at the United States Naval Observatory (USNO) through global positioning system time and the absolute frequency accuracy for experiments is at 1×10^{-13}.

To minimize the optical pumping and ac stark shift, the power of the probe beams is attenuated to the magnitude of a few nW. The transmission of probe beam is set to about 40% by adjusting the optical density of the atoms, which is typically less than 10% of the total atoms involved in the excitations in order to probe the linear response.

Under the condition of very weak probe lights, the optical signal will be buried by noise when detectors are directly used to collect lights. Here we use heterodyne detection to achieve photon shot-noise limited detection of spectroscopy of ^{6}Li, as shown in Fig. 1. The frequency difference between the strong local oscillator (LO) light and probe light is set by 21 MHz. Two silicon resonant photodetectors (RD1 and RD2) with quantum efficiencies η of 85% are used to detect the beat signals. The LO light with power of 600 μW is split into two parts with the same power. One is optically mixed with the forward probe beam at RD1 and another is mixed with the back-forward probe beam at RD2. The voltages from the detectors are then sent to two separate rf mixers, for which a second mixer whose LO drive has a phase offset 90° with respect to the phase of the first mixer's LO drive. By summing the squares of output of the two mixers, we are able to measure the amplitude of the beat signal, which is insensitive to the relative phase. In such heterodyne detections, the contrast C, describing the mode matching between the probe and local beam, is very critical, which has been to approach 100% to reach shot noise limit. In the measurements, the contrast is optimized to be better than 97% (see Supplemental Material [29]). The shot-noise limited performance of our heterodyne detection is illustrated in Fig. 2(a), the noise of the weak beam normalized to the expected shot noise ($\delta_{\mathrm{shot}} = C\sqrt{\eta N_{\mathrm{probe}}}$, where N_{probe} is the photon numbers of the light beam) as a function of the probe pulse duration with a fixed intensity. For a large range of pulse durations from 1 to 100 μs, the normalized noise is very close to 1, the so-called photon shot-noise limit. The small noise of the pulses shorter than 1 μs is caused by the low-pass filter in the measurement system. Noise increases at longer pulse widths due to the slow change of probe light intensity and the drift of the relative phase. In the following frequency measurement, the pulse duration of the weak probe beams is fixed at 200 μs. The typical absorption spectra of the transition $2S_{1/2}$, $F = 3/2 \rightarrow 2P_{1/2}$, $F' = 3/2, 1/2$, and their corresponding fitted profiles are shown in Fig. 2(b). The fitted linewidth of the transition is about 7.37 MHz, 20% greater than the natural linewidth of 5.87 MHz, which is mainly due to the residual Doppler effect. Using the heterodyne detection, SNR is greatly enhanced to approach the shot-noise limit.

In the experiment, the fluctuation of atom numbers has also to be considered. For a single shot, the loss of atoms is below 2% of the total numbers by controlling the intensity,

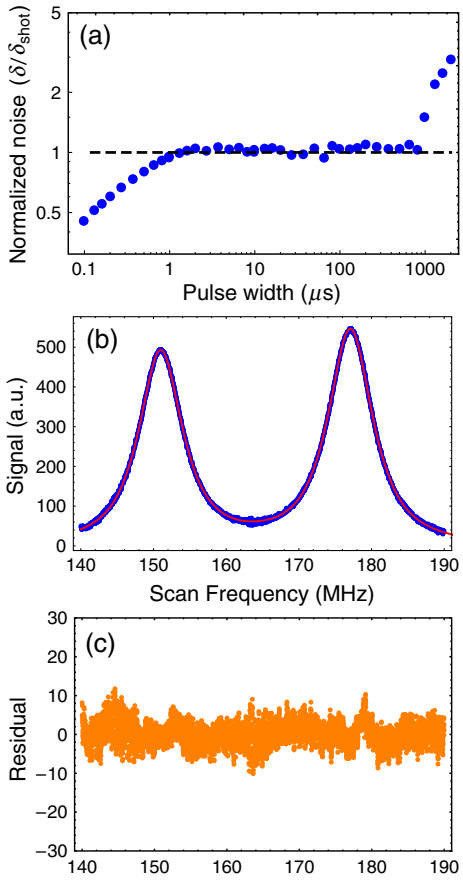

FIG. 2. Optical spectroscopy with photon shot-noise limited detection. (a) Noise of heterodyne detection relative to the expected shot noise as a function of the pulse duration for an LO power of 600 μW and a probe light power 30 nW. The frequency drift and low-pass filter make the heterodyne scheme no longer shot-noise limited at very short and long timescales. (b) Typical data (blue points) of the transition $2S_{1/2}$, $F = 3/2 \rightarrow 2P_{1/2}$, and $F' = 3/2$, $1/2$ and their corresponding fitted profiles (red curves). (c) Fit residual.

the pulse duration, and frequency scanning speed of probe beams. For multiple repeated measurements, the fluctuation of atom numbers between shot to shot is suppressed by the normalization. At the end of the probe, a standard absorption image for cold atoms is performed. The total atom numbers obtained from the image are used to normalize atom number to further reduce the fluctuations. Another contribution of the fluctuation is from an effective optical density (OD), which is determined using $\mathrm{OD} = \log(I_t/I_0)$, where I_t and I_0 are the light intensity of the transmission and incident probe beams, respectively. This fluctuation is very small due to very weak intensity of the probe beam and the isolation of the surrounding mechanical vibrations and acoustical noise.

Although the very low intensity of the probe beams (typically below $10^{-3} I_s$, where I_s is the saturation intensity) and two beams' configuration with equal intensity can compensate for the effect from the atoms motion and spatial

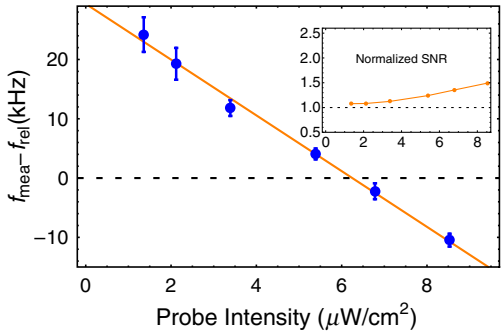

FIG. 3. The measured frequency shift as a function of the probe beam intensity. Blue dots are the measured data and solid line is a linear fit to extract the frequency with zero intensity of probe beams. The error bar is from statistics. Inset is the SNR of the spectroscopy normalized by one predicted by shot noise limited detection.

distribution, the light forces can still cause the observable shift of the measured frequency [33,34]. In the experiment, the frequency shift is positive for a traveling-wave probe and negative for the counterpropagating beams. Figure 3 presents our measured frequency of $2S_{1/2}$, $F = 3/2 \rightarrow 2P_{1/2}$, and $F' = 3/2$ relative to f_{rel} as a function of probe intensity, where $f_{\mathrm{rel}} = 446\,789\,528.716(10)$ MHz is the corresponding transition frequency from a recent NIST measurement [20]. Here each measured frequency is the average of 1000 measurements with the same conditions and each measurement achieves the photon shot-noise limited, as shown in the inset. It is obvious that the frequency shift induced by the probe intensity is not negligible at the level of kHz precision. About a 30 kHz shift is observed when the intensity is changed from 1 to 8 $\mu\mathrm{W/cm}^2$. We obtained f_{rel}, the measured value from NIST, at 6 $\mu\mathrm{W/cm}^2$. The final absolute frequency is obtained by extrapolating the measured value to zero-intensity position with a linear fit.

Our measured frequencies for all hyperfine components and resulting centers of gravity of the D_1 and D_2 lines of ^{6}Li are given in Table I. An uncertainty is determined considering all identified sources of error, which are shown in Table II. The total uncertainty is derived by combining the individual elements in quadrature.

The uncertainty of our measurement of the resolved D_1 lines is smaller than 1 kHz and less than 2.0 kHz for unresolved D_2 lines. The main uncertainty for D_1 lines is from the statistical variation of multiple measurements. The small first residual Doppler uncertainty is due to imperfections of the alignment of two beams and the finite temperature of cold atoms. It should be pointed out that the relative transition strengths of $2S_{1/2}$, $F = 1/2 \rightarrow 2P_{1/2}$, and $F' = 1/2$ is 8 times smaller than $2S_{1/2}$, $F = 1/2 \rightarrow 2P_{1/2}$, and $F' = 3/2$. In order to get the best SNR, the power of probe beams is slightly increased in the measurement, which causes the relative higher uncertainty in the

TABLE I. Measured frequencies of hyperfine components and centers of gravity (COG) of the ^{6}Li D lines.

Line	F_g	F_e	Frequency (MHz)
D_1 $2S_{1/2} \rightarrow 2P_{1/2}$	$F=3/2$	$F'=1/2$	446 789 502.639 3(9)
	$F=3/2$	$F'=3/2$	446 789 528.744 2(9)
	$F=1/2$	$F'=1/2$	446 789 730.842 4(23)
	$F=1/2$	$F'=3/2$	446 789 756.943 9(8)
D_2 $2S_{1/2} \rightarrow 2P_{3/2}$	$F=3/2$	$F'=5/2$	446 799 571.079 6(19)
	$F=3/2$	$F'=3/2$	446 799 573.974 3(19)
	$F=3/2$	$F'=1/2$	446 799 575.686 1(19)
	$F=1/2$	$F'=3/2$	446 799 802.175 8(16)
	$F=1/2$	$F'=1/2$	446 799 803.887 6(16)
D_1 COG			446 789 596.109 4(8)
D_2 COG			446 799 648.889 8(16)

extrapolation, as shown in Table I. Similar to NIST's measurement [20], quantum interference plays an important role for determining the absolute transition frequencies to unsolved D_2 lines (see Supplemental Material [29]). The largest contributors to the uncertainties are inaccuracy in the hyperfine constants [14], which are estimated by holding the line shape parameters and component intensities fixed and letting the A and B constants vary, and the laser power dependent shifts. The frequency shift due to the local field effect is estimated about blueshift 28 Hz for the D_1 line and 57 Hz for the D_2 line by $\Delta_{LL}=-n_0 d^2/(3\epsilon_0\hbar)$ [35], where d is the transition dipole moment, and n_0 is the atom's number density. Other collective effects from scattering are very small due to small atom number density ($n_0 k^{-3} = 3.8\times10^{-6}$) and the weak-driving case. Under low-order approximation, the collectively broadened linewidth depends on the optical density and frequency shift depends on the density [36], which is about 2.3 Hz in the experiment. Other uncertainties, such as optical pumping, multiple excitation photon recoil, and the ac Stark effect are small due to a very weak probe beam and the usage of the intensity extrapolation in our measurement.

The only two previous precise measurements of absolute transition frequencies were reported by Das *et al.* [16] as

TABLE II. Uncertainty budgets (Hz) for the measurement.

Uncertainty component	D_1 lines	D_2 lines
Reference frequency	45	45
Statistical variation	813	1048
First order Doppler	375	375
ac Stark shift	40	10
Magnetic field shift	84	84
Local field shift	−28	−57
Local field variance	3	6
Forward collective scattering	<10	<10
Collision shift	<100	<100
Hyperfine constant inaccuracy	0	1150
Total	906	1606

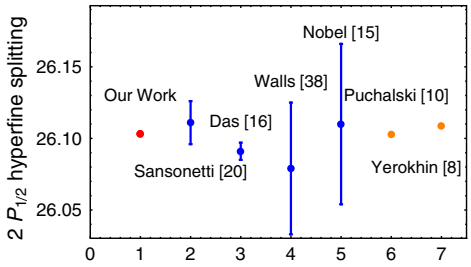

FIG. 4. The comparison of the hyperfine interval of $2P_{1/2}$ state. Red dot is from our measurement, orange dots are for the calculations [7,8], and blue dots are other experiments.

well as Sansonetti *et al.* [20]. The uncertainty of the measurement is about an order of magnitude smaller than the values of the previous most precise results in Ref. [20]. The results presented in Table I disagree with values of Ref. [16] by 20σ to 85σ. The absolute transition frequencies are larger than the corresponding NIST measurements from 2 to 28 kHz for the D_1 lines. These differences may come from the large density induced shift in their measurements. For D_2 lines, our results are consistent with their values at the 1σ level. The comparison of our results for hyperfine intervals with previous results is shown in Fig. 4. When measuring the hyperfine interval of the $2P_{1/2}$ state, we precisely control the frequencies of probe beams with a triangular wave, which scans the probe beams from low to high frequency and high to low frequency, and then average the measured values. By using this method, the systematic errors and uncertainty are further suppressed. The measured $2P_{1/2}$ hyperfine splitting is 26.103 1 (14) MHz, which is in excellent agreement with recent theoretical calculation 26.102 6 (4) MHz [7]. Our results for the ground state hyperfine splittings is 228.201 5(14) MHz, which differs by 2.6σ with atomic beam magnetic resonance results measured by Beckmann [37]. The claimed measured accuracy is at the order of Hz, which is about 3 orders more accurate than the current measurement. The many sources of the systematic errors had to be considered in this level. The measurement and the inconsistency are worth further investigation.

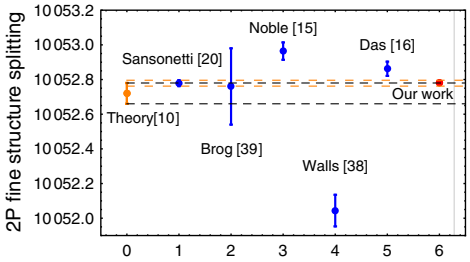

FIG. 5. The comparison for $2P_{3/2}-2P_{1/2}$ fine structure splitting of ^{6}Li. Red dot is from our measurement, orange dot is for the calculations [10], and blue dots are the measured values from other experiments.

Figure 5 is the comparison for $2P_{3/2} - 2P_{1/2}$ fine structure splitting of ^{6}Li. Our measurement is 10 052.780 4 (18) MHz (red point in Fig. 5), which is in agreement with the most recent measurements [20] and theory including $m\alpha^6$ and $m\alpha^7 \ln(\alpha)$ contributions [10,11].

In conclusion, we develop the photon shot-noise limited detection and first measure the transition frequencies in cold atoms of ^{6}Li by using the optical frequency comb. The results are more than an order of magnitude more accurate than previous experiments. The measurements confirm recent calculations of the $2P$ fine splitting including higher order relativistic and QED contributions and help to resolve large disagreements between theory and experiment. We are generalizing such measurements to cold atoms of ^{6}Li and ^{7}Li, which will determine the isotope shifts and relative nuclear charge radius at the higher precision level.

This research is supported by the National Key Research and Development Program of China (Grants No. 2017YFA0304201 and No. 2017YFA0304403), National Natural Science Foundation of China (NSFC) (Grants No. 11925401, No. 11734008, No. 11374101, No. 91536112, and No. 11621404, No. 11822402), and Program of Shanghai Subject Chief Scientist (17XD1401500), and the Shanghai Committee of Science and Technology (17JC1400500), and the Innovation Program of Shanghai Municipal Education Commission (2019-01-07-00-05-E00079).

*ylwu@phy.ecnu.edu.cn
†yyjiang@phy.ecnu.edu.cn
‡hbwu@phy.ecnu.edu.cn

[1] W. Nörtershäuser *et al.*, Phys. Rev. A **83**, 012516 (2011).
[2] G. A. Noble and W. A. van Wijngaaeden, Can. J. Phys. **87**, 807 (2009).
[3] W. A. van Wijngaaeden and B. Jian, Eur. Phys. J. Spec. Top. **222**, 2057 (2013).
[4] Z.-T. Lu, P. Mueller, G. W. F. Drake, W. Nörtershäuser, S. C. Pieper, and Z.-C. Yan, Rev. Mod. Phys. **85**, 1383 (2013).
[5] Z. C. Yan and G. W. F. Drake, Phys. Rev. A **66**, 042504 (2002).
[6] Z. C. Yan, W. Nörtershäuser, and G. W. F. Drake. Phys. Rev. Lett. **100**, 243002 (2008).
[7] M. Puchalski and K. Pachucki, Phys. Rev. A **79**, 032510 (2009).
[8] V. A. Yerokhin, Phys. Rev. A **78**, 012513 (2008).
[9] M. Puchalski, A. M. Moro, and K. Pachucki, Phys. Rev. Lett. **97**, 133001 (2006).
[10] M. Puchalski and K. Pachucki, Phys. Rev. Lett. **113**, 073004 (2014).
[11] L. M. Wang, C. Li, Z.-C. Yan, and G. W. F. Drake, Phys. Rev. A **95**, 032504 (2017).
[12] M. Puchalski, D. Kedziera, and K. Pachucki, Phys. Rev. A **87**, 032503 (2013).
[13] C. J. Sansonetti, B. Richou, R. Engleman, Jr., and L. J. Radziemski, Phys. Rev. A **52**, 2682 (1995).
[14] B. A. Bushaw, W. Nörtershäuser, G. Ewald, A. Dax, and G. W. F. Drake, Phys. Rev. Lett. **91**, 043004 (2003).
[15] G. A. Noble, B. E. Schultz, H. Ming, and W. A. van Wijngaarden, Phys. Rev. A **74**, 012502 (2006).
[16] D. Das and V. Natarajan, Phys. Rev. A **75**, 052508 (2007).
[17] Y. Huang, W. Luo, Y. Kuo, and L. Wang, J. Phys. B **46**, 075004 (2013).
[18] Y. H. Lien, K. J. Lo, H. C. Chen, J. R. Chen, J. Y. Tian, J. T. Shy, and Y. W. Liu, Phys. Rev. A **84**, 042511 (2011).
[19] K. C. Brog, T. G. Eck, and H. Wieder, Phys. Rev. **153**, 91 (1967).
[20] C. J. Sansonetti, C. E. Simien, J. D. Gillaspy, J. N. Tan, S. M. Brewer, R. C. Brown, S. Wu, and J. V. Porto, Phys. Rev. Lett. **107**, 023001 (2011).
[21] R. C. Brown, S. Wu, J. V. Porto, C. J. Sansonetti, C. E. Simien, S. M. Brewer, J. N. Tan, and J. D. Gillaspy, Phys. Rev. A **87**, 032504 (2013).
[22] I. Tanihata, H. Hamagaki, O. Hashimoto, Y. Shida, N. Yoshikawa, K. Sugimoto, O. Yamakawa, T. Kobayashi, and N. Takahashi, Phys. Rev. Lett. **55**, 2676 (1985).
[23] G. Ewald, W. Nörtershäuser, A. Dax, S. Götte, R. Kirchner, H.-J. Kluge, Th. Kühl, R. Sanchez, A. Wojtaszek, B. A. Bushaw, G. W. F. Drake, Z.-C. Yan, and C. Zimmermann, Phys. Rev. Lett. **93**, 113002 (2004).
[24] R. Sanchez *et al.*, Phys. Rev. Lett. **96**, 033002 (2006).
[25] S. Deng, A. Chenu, P. Diao, F. Li, S. Yu, I. Coulamy, A. del Campo, and H. Wu, Sci. Adv. **4**, eaar5909 (2018).
[26] S. Deng, Z. Shi, P. Diao, Q. Yu, H. Zhai, R. Qi, and H. Wu, Science **353**, 371 (2016).
[27] A. T. Grier, I. Ferrier-Barbut, B. S. Rem, M. Delehaye, L. Khaykovich, F. Chevy, and C. Salomon, Phys. Rev. A **87**, 063411 (2013).
[28] Y. Wu, R. Li, Y. Rui, H. Jiang, and H. Wu, Acta Phys. Sin. **67**, 163201 (2018); http://wulixb.iphy.ac.cn/article/id/72678.
[29] See Supplemental Material at http://link.aps.org/supplemental/10.1103/PhysRevLett.124.063002 for the reference frequency accuracy, magnetic field shift, residual Doppler effect, heterodyne detection, and the fit process of the D_2 line, which includes Refs. [30–32].
[30] T. A. Savard, S. R. Granade, K. M. O'Hara, M. E. Gehm, and J. E. Thomas, Phys. Rev. A **60**, 4788 (1999).
[31] J. M. Pino, R. J. Wild, P. Makotyn, D. S. Jin, and E. A. Cornell, Phys. Rev. A **83**, 033615 (2011).
[32] A. Yariv, *Optical Electronics in Modern Communications* (Oxford University Press, New York, 1977).
[33] M. G. Prentiss and S. Ezekiel, Phys. Rev. Lett. **56**, 46 (1986).
[34] M. Artoni, I. Carusotto, and F. Minardi, Phys. Rev. A **62**, 023402 (2000).
[35] H. A. Lorentz, *The Theory of Electrons* (BG Teubner, Leipzig, 1909).
[36] B. Zhu, J. Cooper, J. Ye, and A. M. Rey, Phys. Rev. A **94**, 023612 (2016).
[37] A. Beckmann, K. D. Böklen, and D. Elke, Z. Phys. **270**, 173 (1974).
[38] J. Walls, R. Ashby, J. Clarke, B. Lu, and W. van Wijngaarden, Eur. Phys. J. D **22**, 159 (2003).
[39] K. C. Brog, T. G. Eck, and H. Wieder, Phys. Rev. **153**, 91 (1967).